RESEARCH ARTICLE

# Adsorption study of Ni (II) ion and azo dye DR278 in aqueous media using $MoS_2$/O-MWCNTs adsorbent and optimization by response surface methodology

***Elham Ahangaran[1], Hossein Aghaie[2,*], Reza Fazaeli[3]***

[1]*Department of Chemistry, Science and Research Branch, Islamic Azad University, Tehran, Iran*

[2] *Department of Chemistry, Science and Research Branch, Islamic Azad University, Tehran, Iran*

[3]*Department of Chemical engineering, Faculty of engineering, South Tehran Branch, Islamic Azad University, Tehran, Iran*

**ARTICLE INFO**

***Article History:***
*Received 2022-05-27*
*Accepted 2024-06-12*
*Published 2023-09-15*

***Keywords:***
*$MoS_2$, O-MWCNTs,*
*Adsorption, DR278,*
*Ni (II),*
*Kinetics,*
*Thermodynamic,*
*water treatment*

**ABSTRACT**

In this research, molybdenum disulfide ($MoS_2$) particles were synthesized by the hydrothermal method and loaded on oxidized multiwalled carbon nanotubes (O-MWCNTs). $MoS_2$ and $MoS_2$/O-MWCNTs particles were characterized by several techniques. Adsorption of Direct Red 278 (DR278) and Ni (II) ions was investigated onto $MoS_2$ and $MoS_2$/O-MWCNTs particles. The effect of adsorbent mass (g), contact time (min), and pH was evaluated by response surface methodology (RSM). The software determined the best point to achieve the highest removal efficiency for azo dye DR278, in the optimal conditions of adsorbent mass 0.03 (g), contact time 27.54 (min), and pH 5.01, 99.99%. Also, the removal efficiency for Ni (II) ion, under optimal conditions of adsorbent mass 0.04 (g), time 26.61 (min) and pH 7.09, 97.83%. Isothermal studies showed that the Dubinin–Radushkevich model had the highest correlation coefficients of 0.98 and 0.97 for Ni (II) ion and azo dye DR278 with the respectively lowest error rate, and the highest correlation to the experimental data. The adsorption kinetic results showed ion Ni (II) ion and Azo dye DR278 adsorptions are well described by the mentioned adsorbent with pseudo-second order kinetic model.

**How to cite this article**

*Ahangaran E., Aghaie H., Fazaeli R., Adsorption study of Ni (II) ion and azo dye DR278 in aqueous media using MoS2/O-MWCNTs adsorbent and optimization by response surface methodology. J. Nanoanalysis., 10 (3): 560-577, Summer 2023.*

*Corresponding Author Email: *hn_aghaie@yahoo.com & h.aghaie@srbiau.ac.ir*

**INTRODUCTION**

One of the most important issues in the world today is the pollution of the environment with toxic and dangerous metal ions. The extraction of metals from mines and the widespread use of heavy metals in industry have caused the concentration of ions of these metals in water, wastewater, air, and soil to increase more than the baseline values. The environmental hazards posed by the deposition of heavy metals in the soil have been highly toxic to humans, even at low concentrations, and have been a major concern in recent years [1-3]. Pigment-containing industrial effluents are usually discharged directly into adjacent waterways, rivers, lagoons, and lakes, causing damage to the receiving waters, the ecosystem of aquatic organisms, and the biological species of the environment [4, 5]. Effluents containing organic dyes that are released onto the surface of the receiving water are toxic compounds whose concentration is higher than the concentration threshold of aquatic organisms. Azo dye wastewater is one of the main problems of the textile dyeing industry, which not only damages the beauty of nature and its surroundings but also causes toxicity to aquatic habitats and can affect the human food cycle [6-10]. One of the most important and widely used dyes in the textile industry is Direct Red 278. Due to the presence of aromatic bases, these dyes have potentially carcinogenic and mutagenic properties and are also resistant to environmental biodegradation. Due to the lack of water and the occurrence of environmental problems caused by the discharge of sewage and effluents into the receiving water, wastewater treatment and the possibility of reusing it has been considered. This operation is performed using physical, chemical, and biological processes and continues until the quality of the effluent reaches the level of existing standards [11, 12]. The study of the adsorption of environmental pollutants is considered from various aspects, and many studies have been done in this field; therefore, it is intended to study the removal of some pharmaceutical, ionic, and dye pollutants through adsorption. This method can remove many environmental pollutants, such as drugs, dyes, or ions that are present in industrial effluents [13, 14]. The waste water treatment processes are ion exchange [15], membrane filtration [16], solvent extraction [17], electrochemical methods [18], chemical precipitation [19], adsorption [20], biological [21], photocatalysis [22-25] and Fenton oxidations [26]. Adsorption is the process of accumulating substances in a boron solution in a common phase. In other words, adsorption is a mass transfer operation in which a component in the liquid phase is transferred to the solid phase. The adsorbent is a substance that is removed from the liquid in a common phase. Absorbent waves may also have a solid, liquid, or gaseous phase on which the adsorbent accumulates [20]. Carbon nanotubes are one of the new adsorbents in the field of nanotechnology, which has studied the removal efficiency of environmental pollutants in various studies [20]. Carbon nanotubes are actually plates of carbon atoms that move inside a roller-like part. High specific surface area, excellent reactivity, abundant thermal and mechanical resistance, and unique chemical, electrical, and physical properties are among the characteristics of these materials. Single-walled carbon nanotubes have a smaller diameter and length than multi-walled carbon nanotubes and cannot be mass-produced due to their small size. But they are easier to use than multi-walled carbon nanotubes [27]. In recent years, nanomaterials have been considered by many researchers due to their unique physical and chemical properties. Among these nanomaterials are a family of chemical compounds known as dicalcogen-mediated metals that have shown interesting properties. $MOS_2$ is part of the family of dicalcogen intermediate metals. Unlike graphene, these materials offer a variety of electronic properties. As the most famous member of the family of intermediate dicalcogenes, $MoS_2$ has been extensively used in two-dimensional fields in various fields such as

biomedicine, sensing, catalytic, and field-effect transistors. However, the introduction of new methods for the synthesis of 2D $MoS_2$ nanosheets as well as the improvement of existing synthesis methods is considered one of the main challenges [28, 29]. Recently, the use of $MoS_2$ nanostructures as an adsorbent in aqueous solutions; especially with the nanosheet structure, has received a lot of attention [30]. Meanwhile, the preparation of molybdenum disulfide nanostructures by various methods of preparing nanostructures in parallel with their application has received much attention. One of the most optimal methods for the production of nanostructures is the hydrothermal method. In this study, $MoS_2$ particles were synthesized by the hydrothermal method and loaded on O-MWCNTs. The RSM with BBD was used to investigate the effects of factors and process optimization with Design Expert software. The effect of adsorbent mass (g), time (min), and pH was evaluated at three levels. Also isothermic and kinetic.

## MATERIAL AND METHODS

*Material*

Ammonium heptamolybdate tetrahydrate ($(NH_4)_6Mo_7O_{24}$, $\geq$ 99%), thiourea ($CH_4N_2S$, > 99%), carbon nanotubes, multi-walled (MWCNTs), and nickel (II) nitrate hexahydrate ((Ni $(NO_3)_2.6H_2O$) 99.99%) from Sigma-Aldrich Company were prepared. Direct Red 278 was purchased from Colorant Limited Company. The chemical structure of DR 278 is shown in Figure 1.

*$MoS_2$ particle synthesis*

First, 1.24 g of $(NH_4)_6Mo_7O_{24}$ was dissolved in 18 mL of distilled water and placed on a magnetic stirrer (Solution I). Next, 2.28 g of $CH_4N_2S$ was added to 18 mL of distilled water and placed on a magnetic stirrer (Solution II). Solution II was added dropwise to Solution I. The resulting solution was placed in an autoclave of stainless steel for 7 hours at a temperature of 180 °C. The resulting precipitate was washed several times with distilled water and heated in an oven at 150 °C for 2 hours to give the $MoS_2$ product.

The following reaction formula for $MoS_2$ particle synthesis was suggested to be involved during the whole conversion process:

$$2(NH_4)6Mo_7O_{24}.4H_2O + 28CH_4N_2S + 14H_2O \rightarrow 14MoS_2 + 28CO_2 + 68NH_3 + 7O_2 \quad (1)$$

*Synthesis of $MoS_2$/O-MWCNTs particles*

0.5, 1, and 2 g of $MoS_2$ were added to 50 mL of distilled water and placed on a magnetic stirrer (Solution I). 1 g of O-MWCNTs was added to 50 mL of distilled water and placed on a magnetic stirrer (Solution II). Solution II was added dropwise to Solution I. The resulting mixture was stirred for 24 hours without heating. The resulting precipitate was heated in an oven at 150 °C for 2 hours.

*Adsorption of azo dye DR 278 by adsorbents*

50 mL of Azo dye DR 278 solution was prepared at a concentration of 100 mg/L at neutral pH, and then fill them with 0.01 g of O-MWCNTs, $MoS_2$, and $MoS_2$/O-MWCNTs adsorbents in weight ratios of 1:1, 2:1, and 1:2, pour into an Erlenmeyer flask, and place on a shaker at 200 rpm for 30 min. Finally, the solutions were then centrifuged and analyzed by a UV-Vis spectrophotometer at a maximum absorbance of 456 nm.

If $A_0$ and $A_e$ are the initial absorption and equilibrium adsorption in solution, respectively, the adsorption percentage, can be determined through the equations 2:

$$\text{Adsorption}\% = \frac{(A_0 - A_i)}{A_0} \times 100 \quad (2)$$

The equilibrium adsorption capacity $q_e$ of $MoS_2$-O-MWCNTs per gram in mg of adsorbate at equilibrium, $q_e$ (mg/ g), can be determined through the equation 3:

$$q_e = \frac{V(C_0 - C_e)}{W} \quad (3)$$

$q_e$ is the equilibrium adsorbent capacity (mg/g), $C_0$ is the initial adsorption concentration in the solution (mg/L), Ce is the equilibrium adsorption concentration in the solution (mg/L) in equilibrium, V is the volume of the adsorbent solution in liters (L) and W is the weight of the adsorbent in terms of (g).

*Adsorption of Ni (II) by adsorbents*

Prepare 50 mL of Ni (II) solution at a concentration of 100 mg/L at neutral pH and then fill them with 0.01 g of O-MWCNTs, $MoS_2$, and $MoS_2$/O-MWCNTs adsorbents in weight ratios of 1:1, 2:1, and 2:1. Pour into an Erlenmeyer flask and shake at 200 rpm for 30 minutes. The desired solutions were then centrifuged and analyzed by ICP-OES.

*Design of experiment by response surface methodology*

The response surface methodology (RSM) summarizes the use of mathematical methods and statistical techniques to construct experimental models of the process under study [31- 33]. In these methods, in addition to the main effects between factors, it is possible to estimate the interactive effects and interactions between factors. The RSM is easily accessible and examined by examining the interactions between the factors. Box-Behnken design (BBD) is an incomplete three-level factor design. In this method, a block of two-level experiments is repeated between different sets of variables. This scheme was presented to solve the problem of a large number of experiments in design with a large number of factors. The number of experiments is kept constant so that it is sufficient to estimate the coefficients of the quadratic equation.

In this study, the RSM with BBD with 3 variables was used to investigate the relationship between the obtained responses and process variables and optimize the combinations with Design Expert software. In this study, the effect of adsorbent mass (g), time (min) and pH was evaluated at 3 levels for the azo dye DR278 and Ni (II) ions (Table 1). To achieve the optimal design conditions, the experiment was performed as a function of the main parameters. The behavior of the system can be explained using the quadratic equation.

The general response surface equation is defined as follows:

$$Y = \beta_0 + \sum_{j=1}^{k} \beta_j X_j + \sum_{j=1}^{k} \beta_{jj} X_j^2 + \sum_i \sum_{<j=2}^{k} \beta_{ij} X_i X_j + e_i \quad (4)$$

In this equation, $x_i$ and $x_j$ are independent variables, $\beta_0$ is a constant coefficient, $\beta_j$, $\beta_{jj}$ and $\beta_{ij}$ are linear coefficients, quadratic coefficients and interaction sentences, respectively.

*Adsorption isotherm studies*

Adsorption equilibrium data were analyzed by Langmuir, Freundlich, Tamkin, and Redlich-Peterson adsorption isotherm models for $MoS_2$/O-MWCNTs for Ni (II) ion and DR278 dye, and the amount of adsorbed qe (mg/g) per adsorbent mass unit was calculated. Then, using curve expert software, equilibrium concentration and absorption capacity numbers were used to obtain the unknowns of isothermal equations and to calculate computational $q_e$ [34-36].

*Adsorption kinetics studies*

In this study, pseudo-first-order and pseudo-second-order and intraparticle diffusion control kinetic models, were used to investigate the adsorption of Ni (II) ions and azo dye DR 278 by the adsorbent $MoS_2$/O-MWCNTs (1:1). Kinetic equations examine the rate at which chemical changes in a substance change over time. Equilibrium constants and kinetic constants can be determined using kinetic equations.

To investigate the kinetics of Ni (II) ion adsorption by $MoS_2$/O-MWCNTs (1:1) adsorbent, 0.04 g of adsorbent was poured into 50 mL of Ni (II) at a concentration of 100 mg/L at pH 7, and at times of 5, 10, 15, 20, 25, and 30 min, their absorption was found by ICP-OES, and the absorption capacity was calculated at the mentioned time $q_t$.

To investigate the kinetics of azo dye DR 278 adsorption by $MoS_2$/O-MWCNTs (1:1) adsorbent, 0.03

g of adsorbent was poured into 50 mL of azo dye DR 278 at a concentration of 100 mg/L at pH 7, and at times 5, 10, 15, 20, 25, and 30 min were sampled, and finally, their absorption was found by UV-Vis spectrophotometer at a maximum absorbance of 456 and the absorption capacity was calculated at the mentioned time $q_t$.

Using the obtained $q_e$ and $q_t$ and the desired kinetic equations, the adsorption kinetics of Ni (II) ion and azo dye DR 278 on the $MoS_2$/O-MWCNTs (1:1) adsorbent were evaluated.

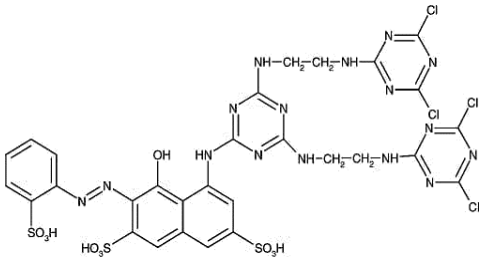

**Figure 1.** Chemical Structure of DR 278.

**Table 1.** Independent variables and their levels in the experimental

| Independent Variables | Coded Symbols | Levels |
|---|---|---|
| Mass of adsorbent (g) | $X_1$ | 0.01 0.03 0.05 |
| Time (min) | $X_2$ | 5 17.5 30 |
| pH | $X_3$ | 5 7 9 |

## RESULTS AND DISCUSSIONS

The X-ray diffraction (XRD) technique was used to identify the phase and structure of $MoS_2$ and $MoS_2$/O-MWCNTs adsorbents. Figure 2a) shows the XRD pattern of $MoS_2$ and $MoS_2$/O-MWCNTs adsorbents. The comparison of the X-ray diffraction spectra of $MoS_2$ and $MoS_2$/O-MWCNTs adsorbents in Figure 2 shows that $MoS_2$ is well loaded on O-MWCNTs. The XRD of $MoS_2$ at the angles of 14.39, 32.91, 39.69, and 76.58° correspond to plates (002), (100), (103), and (110), respectively. It indicates the hexagonal phase is in accordance with the standard peaks of the characteristic $MoS_2$ with JCPDS card number 1492-37. The peaks of $MoS_2$/O-MWCNTs at angles 24 and 43° are related to O-MWCNTs, and the peaks at angles 14.39, 32.91, 69.39, and 76.58, respectively, correspond to the plates (002), (100), (103), and (110) correspond to the standard peaks of the characteristic $MoS_2$ with the JCPDS card number No. 1492-37. The average particle size was estimated based on the Debye-Scherrer equation using X'pert Highscore software.

$$B = \frac{K\lambda}{Lcos\theta} \quad (5)$$

where B is the particle size, K is a constant number equal to 0.9, λ is the applied wavelength in terms of nanometers, L is the peak full width at half maximum (FWHM) in terms of radians, and θ is the angle corresponding to the highest peak. The mean particle sizes calculated by the Debye-Scherrer method were $MoS_2$ and $MoS_2$/O-MWCNTs 76.12 and 82.09, respectively.

The interaction of infrared radiation with a sample changes the vibrational energy of the bond in its molecules and is a good way to identify functional groups and molecular structure. The peaks below 700 $cm^{-1}$ reveal the Mo-O deformation mode, possibly caused by the sulfidation vibrations. The peaks

between 750 and 1000 $cm^{-1}$ indicate the most definite information on Mo-O coordination. The absorption band between 1100 and 1650 $cm^{-1}$ is ascribed to the stretching vibrations of the hydroxyl group and Mo-O vibrations. The Mo-S vibration peak is around 500 $cm^{-1}$. The C=C symmetric and asymmetric stretching vibrations are at 2985 and 3148 $cm^{-1}$, which show small changes in energies, and in the peak range of 3424.21 $cm^{-1}$ assigned to the O-H tensile vibration. The spectra of FTIR $MoS_2$/O-MWCNTs in the range of 476.29 $cm^{-1}$ related to the tensile vibration of Mo-S, in the range of 422.49 $cm^{-1}$ characteristic of the C-S bond, in the range of 906.39 $cm^{-1}$ related to S-O-C, in the range of 1114.13, 1405.29, and 1613.36 $cm^{-1}$ correspond to the C-O-H, C=C, and C=O bonds. Also, in the peak range of 3424.21 $cm^{-1}$, it is related to O-H tensile vibration (Figure 2 b). FESEM analysis was used to evaluate the morphology and particle size of $MoS_2$ and $MoS_2$/O-MWCNTs adsorbents. Figure 3 shows the $MoS_2$ and $MoS_2$/O-MWCNT adsorbents. Based on the morphological results, $MoS_2$ is like a flower, and $MoS_2$ particles are well stabilized on O-MWCNTs. Energy-dispersive X-ray spectroscopy (EDS) was used to analyze the surface layers and perform elemental analysis of $MoS_2$/O-MWCNT nanoparticles, which confirmed the presence of C (66.17%), S (9.27%), O (7.78%), and Mo (16.77%) elements (Figure 4). According to Figure 5, in the thermal gravimetric curve (TGA) of the $MoS_2$ sample, there is a 10% weight loss from 220 to 380 $^oC$, which could be related to the degradation of the $MoS_2$ structure. In the TGA of $MoS_2$/O-MWCNTs, a 5% weight loss from 220 to 330 °C and a 10% weight loss from 400 °C to about 800 °C can be observed, which could lead to thermal degradation of carbon graphite structures in O-MWCNTs. $N_2$ adsorption-desorption isotherms of $MoS_2$ and $MoS_2$/O-MWCNTs samples using the BET/BJH method are shown in Figure 6. According to the IUPAC contract, these isotherms are in the type (IV) isotherm group for mesoporous materials with hysteresis loops in the range of $0.6<p/p_o<1$. Based on the results, the surface area of $MoS_2$ is 9.67 ($m^2$/g) but with the loading of O-MWCNTs, the surface area of the adsorbent increased to 125.72 ($m^2$/g). Also, the total pore volume of $MoS_2$ adsorbent increased from 10.58 to 129.41 ($cm^3\ g^{-1}$) after loading on O-MWCNTs (Table 2).

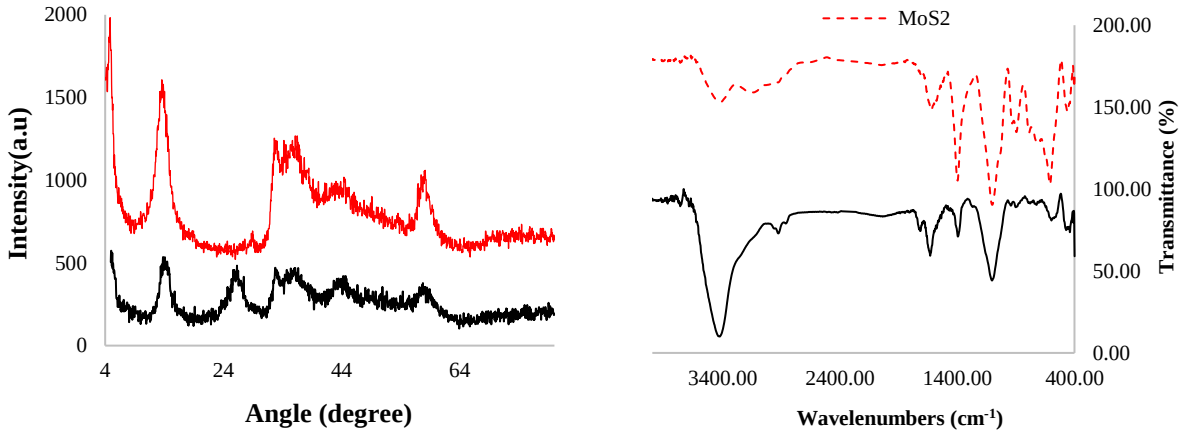


(a) (b)

**Figure 2.** $MoS_2$ and $MoS_2$/O-MWCNTs: **a)** XRD spectra and **b)** FTIR spectra

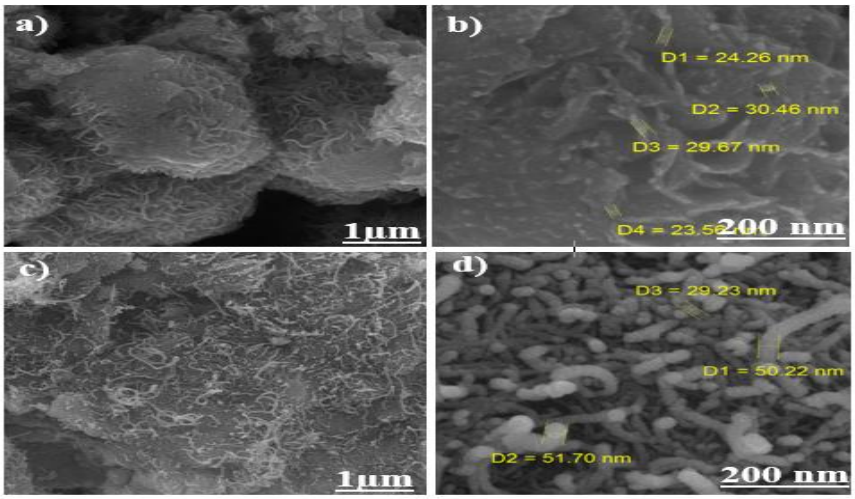


**Figure 3.** SEM images, a) and b) $MoS_2$ and c) and) d $MoS_2$/O-MWCNTs

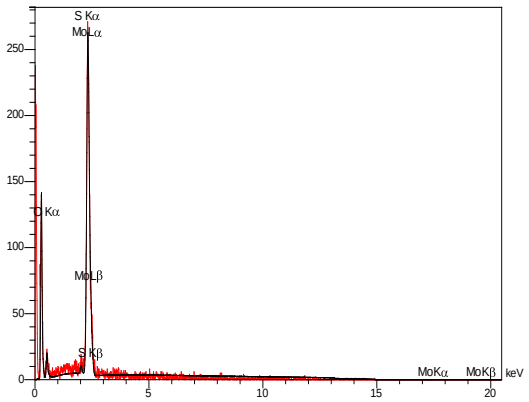


**Figure 4.** EDS pattern of $MoS_2$/O-MWCNTs

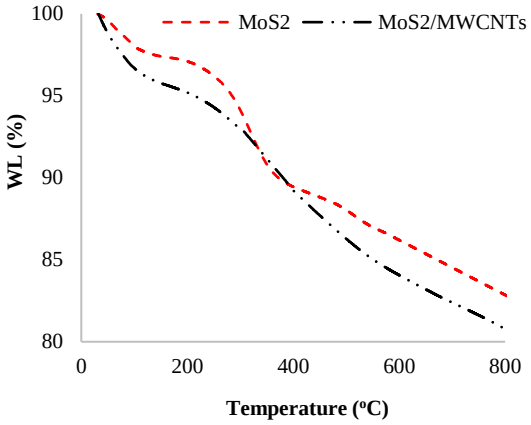


**Figure 5.** TGA results for $MoS_2$ and $MoS_2$/O-MWCNTs

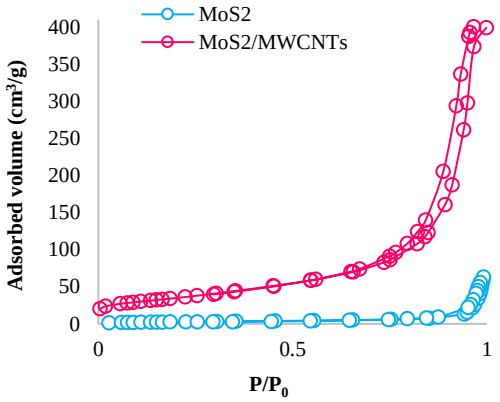


**Figure 6.** BET/BJH analysis for $MoS_2$ and $MoS_2$/O-MWCNTs

**Table 2.** BET/BJH results for $MoS_2$ and $MoS_2$/O-MWCNTs.

| Sample | $S_{BET}$ ($m^2$/g) | Total pore volume ($cm^3$ $g^{-1}$) | Mean pore diameter (nm) |
|---|---|---|---|
| $MoS_2$ | 9.67 | 10.58 | 37.60 |
| $MoS_2$/O-MWCNTs | 125.72 | 129.41 | 19.29 |

*Adsorption of Ni (II) ion and azo dye DR278 by adsorbents:*

In order to investigate the effect of $MoS_2$ loading on O-MWCNTs and their weight ratio in Ni (II) and DR278 removal efficiencies, experiments were performed under the same conditions. The results of Ni (II) and DR278 adsorption by O-MWCNTs, $MoS_2$ and $MoS_2$/O-MWCNTs adsorbents are shown in Table 3. Based on the results, the adsorption efficiency of $MoS_2$ and $MoS_2$/O-MWCNTs is higher than that of $MoS_2$. Also, the highest efficiency related to the weight ratio of 1:1 $MoS_2$ to $MoS_2$/O-MWCNTs was obtained.

*Results of response surface methodology*

In this research, RSM based on BBD with 3 variables was used to investigate the relationship between the obtained responses and process variables and optimize the combination of variables with Design Expert software. The effect of independent variables of adsorbent mass (g), time (min), and pH was investigated at 3 levels for adsorption Ni (II) and DR278.

*Design of experiment of DR 278 dye adsorption:*

The design of the experiment and the results of DR 278 dye adsorption with the RSM based on BBD are shown in Table 4. According to the experimental conditions provided by the software, the highest percentage of azo dye DR278 adsorption was 99.99% by $MoS_2$/O-MWCNTs (1:1) adsorbent. Statistical assumptions are the basis of many univariate and multivariate statistical tests. An essential set of basic conditions for analyzing multivariate data are the presuppositions of normality, linearity, and uniform data scattering. If one or more of these assumptions are ignored, bias or distortion occurs in the statistical results. Being normal is the most basic premise of multivariate analysis. If this assumption is not met, some specific statistical tests are invalid and unusable. Figure 7 a) shows the assumption that the data are normal, that the data are almost normal, and that the results show how the residues follow a normal distribution. This shows a very good correlation between the results obtained by the experimental method and the predicted values by the statistical method. Analysis of variance (ANOVA) is a set of statistical models that examines the mean in groups and their related functions. In this method, the variance obtained from a random variable is divided into smaller components that are the sources of variance. Variance is an indicator for measuring scatter, which shows how much data is scattered above average. Larger values of variance indicate greater dispersion. The square variance is the standard deviation. In Table 5, the desired model, which is the quadratic, is significant, which indicates that the selected model is a suitable model for the data. R-squared is a statistical measurement of data close to the fitted regression line. An important difference between R-Squared and Adj. R-Squared is that R-squared assumes that each independent variable observed in the model explains the changes in the dependent variable. Therefore, the percentage shown by R-Squared assumes the effect of all independent variables on the dependent variable. If the percentage shown by Adj. R-Squared is only the result of the actual effect of the model independent variables on the dependent and not all the independent variables. According to the ANOVA part, the values of R-Squared and Adj. R-Squared were obtained to be equal to 0.9960 and 0.9888, respectively, which is almost close to one and indicates the accuracy of the model. Among the factors, pH (C), adsorbent mass (A), and time (B) had the most effect, respectively (Figure 7b).

**Table 3.** Adsorption of Ni (II) ion and azo dye DR278 by $MoS_2$ and $MoS_2$/O-MWCNTs adsorbents

| Adsorbent | Mass of adsorption (g) | Time (min) | pH | Adsorption (%) |
|---|---|---|---|---|
| O-MWCNTs | 0.01 | 30 | 7 | 72.01 (DR 278) |
| $MoS_2$ | 0.01 | 30 | 7 | 70.54 (DR 278) |

| | | | | |
|---|---|---|---|---|
| $MoS_2$/O-MWCNTs (1:1) | 0.01 | 30 | 7 | 83.43 (DR 278) |
| $MoS_2$/O-MWCNTs (1:2) | 0.01 | 30 | 7 | 79.32 (DR 278) |
| $MoS_2$/O-MWCNTs (2:1) | 0.01 | 30 | 7 | 73.74(DR278) |
| O-MWCNTs | 0.01 | 30 | 7 | 63.24 (Ni(II)) |
| $MoS_2$ | 0.01 | 30 | 7 | 61.17 (Ni(II)) |
| $MoS_2$/O-MWCNTs | 0.01 | 30 | 7 | 75.32 (Ni(II)) |
| $MoS_2$/O-MWCNTs (1:2) | 0.01 | 30 | 7 | 69.01(Ni(II)) |
| $MoS_2$/O-MWCNTs (2:1) | 0.01 | 30 | 7 | 64.32(Ni(II)) |

**Table 4.** The BBD for the 4 independent variables.

| STD | Run | Mass of adsorption (g) | Time (min) | pH | Removal DR (%) |
|---|---|---|---|---|---|
| 11 | 1 | 0.03 | 5.00 | 9.00 | 58.23 |
| 12 | 2 | 0.03 | 30.00 | 9.00 | 68.09 |
| 4 | 3 | 0.05 | 30.00 | 7.00 | 84.52 |
| 6 | 4 | 0.05 | 17.50 | 5.00 | 98.99 |
| 10 | 5 | 0.03 | 30.00 | 5.00 | 99.99 |
| 13 | 6 | 0.03 | 17.50 | 7.00 | 81.33 |
| 7 | 7 | 0.01 | 17.50 | 9.00 | 53.04 |
| 9 | 8 | 0.03 | 5.00 | 5.00 | 95.99 |
| 14 | 9 | 0.03 | 17.50 | 7.00 | 82.12 |
| 8 | 10 | 0.05 | 17.50 | 9.00 | 61.35 |
| 15 | 11 | 0.03 | 17.50 | 7.00 | 80.32 |
| 1 | 12 | 0.01 | 5.00 | 7.00 | 70.92 |
| 3 | 13 | 0.01 | 30.00 | 7.00 | 83.43 |
| 5 | 14 | 0.01 | 17.50 | 5.00 | 94.11 |
| 2 | 15 | 0.05 | 5.00 | 7.00 | 84.22 |

**Table 5.** Results of analysis of variance in DR278

| Source | Sum of squares | Degree of freedom | Mean square | F-value | P-value Prob >F |
|---|---|---|---|---|---|
| Model | 3031.32 | 9 | 336.81 | 138.22 | < 0.0001 significant |
| A-Mass of Adsorbent | 95.08 | 1 | 95.08 | 39.02 | 0.0015 |
| B-Time | 88.91 | 1 | 88.91 | 36.49 | 0.0018 |
| C-pH | 2751.71 | 1 | 2751.71 | 1129.26 | < 0.0001 |
| AB | 37.27 | 1 | 37.27 | 15.30 | 0.0113 |
| AC | 2.94 | 1 | 2.94 | 1.21 | 0.3220 |
| BC | 8.58 | 1 | 8.58 | 3.52 | 0.1193 |
| A2 | 16.18 | 1 | 16.18 | 6.64 | 0.0496 |
| B2 | 9.56 | 1 | 9.56 | 3.92 | 0.1045 |
| C2 | 19.38 | 1 | 19.38 | 7.95 | 0.0371 |
| Residual | 12.18 | 5 | 2.44 | | |
| Lack of Fit | 10.56 | 3 | 3.52 | 4.32 | 0.1936 |
| Pure Error | 1.63 | 2 | 0.81 | | not significant |
| Cor Total | 3043.51 | 14 | | | |

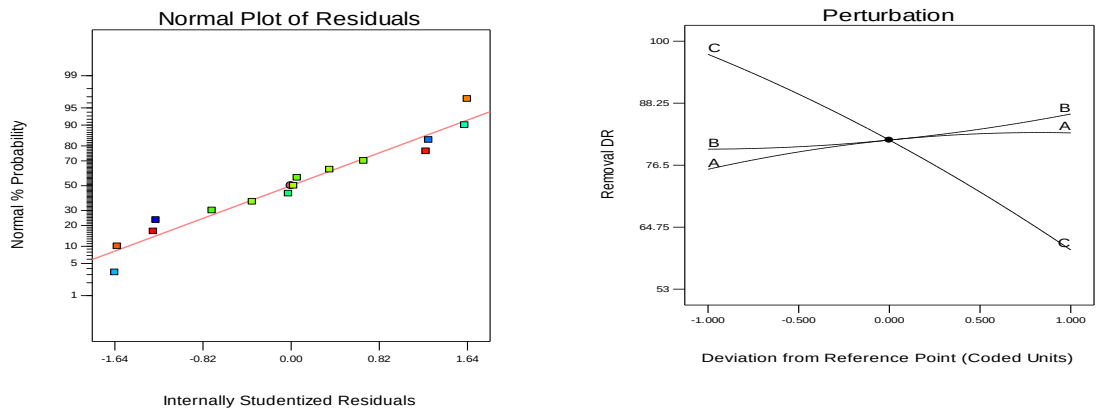


**Figure 7 a)** Normal probability plot of the studentized residual adsorption azo dye DR 278, **b)** Perturbation plot for adsorption azo dye

*The effect of adsorbent mass and time on the adsorption DR 278:*

At this stage of the experiments, the effect of simultaneous changes in the two parameters of adsorbent mass and time on the efficiency of DR278 removal was investigated by considering the dye concentration of DR278 at 10 mg/L. Figure 8a and Figure 8b show the effect of adsorbent mass and time on DR278 dye removal (2D and 3D). Based on the results, the removal efficiency increases with increasing adsorbent mass and time. These results show that the $MoS_2$/O-MWCNTs adsorbent is able to remove DR278 dye from waste water in a shorter time than other adsorbents. Experiments show that due to the significant effective surface of $MoS_2$/O-MWCNTs adsorbent, it has a significant efficiency, and it can be said with confidence that this amount of adsorbent has the ability to remove more than 90% of dye at concentrations of 100 mg/L.

*The effect of adsorbent mass and pH on the adsorption DR 278*

The pH value plays an important role in the adsorption of azo dye by the $MoS_2$/O-MWCNT adsorbent. The surface charge of the particles depends on the pH; therefore, pH is one of the most important control parameters of the adsorption process. The pH affects the reaction between the adsorbent and the adsorbate by changing the azo dye and charging the adsorbent surface. Figure 8c and Figure 8d show the effect of adsorbent mass and pH on the removal of DR278 dye in 2D and 3D. $MoS_2$/O-MWCNTs adsorbents have a higher ability to remove DR278 dye in the acidic pH range and in the range of 5. The surface charge of the $MoS_2$/O-MWCNTs adsorbent becomes more negative with increasing pH, which in turn causes electrostatic reactions. As a result, the negatively charged azo dye will be less adsorbed. When the pH of the solution is lower than $pH_{PZC}$ under acidic conditions, a positive charge is formed on the adsorbent surface, which is effective in the adsorption of anionic species, so it can be concluded that negatively charged organic matter such as DR278 dye in acidic conditions is well absorbed by the adsorbent.

*The effect of time and pH*

Figure 8e and Figure 8f show the effect of time and pH on DR278 dye removal in 2D and 3D. Based on the results, the DR278 dye removal efficiency increases with increasing time and decreasing pH, as shown in Figure 12. In the early stages, the adsorption rate is so high that more than 90% of the DR278 dye is removed from the solution within 5 min, and the experiments lasted up to 30 min, and the results showed that the adsorption capacity did not increase over time. At pHs 5, 7, and 9 the zeta potentials for the adsorbent are -11.3, -14.8, and -21.2 mV, respectively.

*Determining the optimal conditions of adsorption DR 278*

Finally, the software determined the best point to achieve the highest dye removal efficiency of DR278, in optimal conditions with an adsorbent mass of 0.03 g, a time of 27.54 min, and a pH of 5.01, 99.99%. Also, in the optimal conditions obtained, the experiment was performed, and DR278 paint removal efficiency was 99.95% (Figure 9).

*Design of experiment of Ni (II) adsorption*

The results of the design of the experiment Ni (II) adsorption with the RSM based on BBD are shown in Table 6. According to the experimental conditions provided by the software, the highest percentage of 97.43% Ni (II) ion removal was obtained by $MoS_2$/O-MWCNTs adsorbent.

Figure 10a shows the assumption that the data are normal, that the data are almost normal, and that the results show how the residues follow a normal distribution. This shows a very good correlation between the results obtained by the experimental method and the predicted values by the statistical

method. In Table 7, the desired model, which is the quadratic, is significant, which indicates that the selected model is a suitable model for the data. According to the ANOVA part, the values of R-squared and Adj. R-Squared were obtained to be equal to 0.9932 and 0.9810, respectively, which is almost close to one and shows the accuracy of the model. Among the factors, pH, time (B), and adsorbent mass (A) had the most effect, respectively (Figure 10 b).

*Design of experiment of Ni (II) adsorption*

The results of the design of the experiment Ni (II) adsorption with the RSM based on BBD are shown in Table 6. According to the experimental conditions provided by the software, the highest percentage of 97.43% Ni (II) ion removal was obtained by $MoS_2$/O-MWCNTs adsorbent.

Figure 10a shows the assumption that the data are normal, that the data are almost normal, and that the results show how the residues follow a normal distribution. This shows a very good correlation between the results obtained by the experimental method and the predicted values by the statistical method. In Table 7, the desired model, which is the quadratic, is significant, which indicates that the selected model is a suitable model for the data. According to the ANOVA part, the values of R-squared and Adj. R-Squared were obtained to be equal to 0.9932 and 0.9810, respectively, which is almost close to one and shows the accuracy of the model. Among the factors, pH, time (B), and adsorbent mass (A) had the most effect, respectively (Figure 10 b).

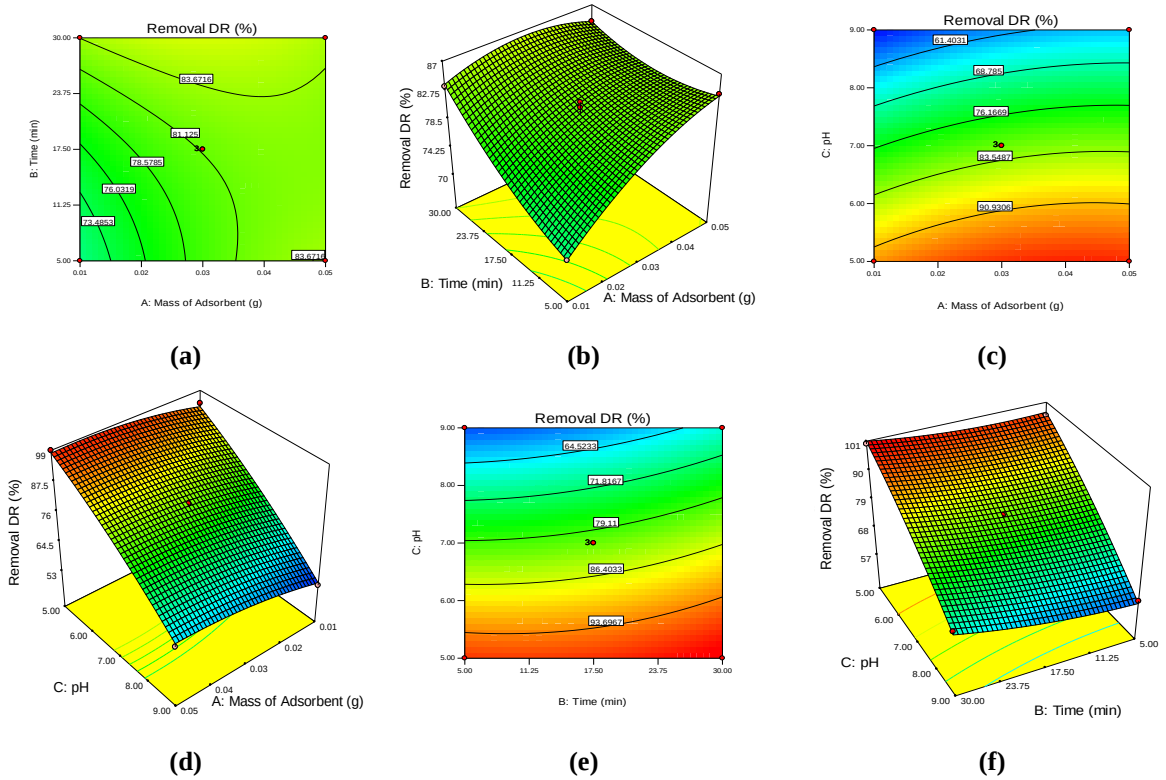


**Figure 8.** The effect of mass of adsorbent and time for adsorption azo dye DR 278 a) Contour and b) 3D plot, the effect of time and pH for adsorption azo dye DR 278 e) Contour and f) 3D plot and the effect of mass of adsorbent and pH for adsorption azo dye DR 278 c) Contour and d) 3D plot.

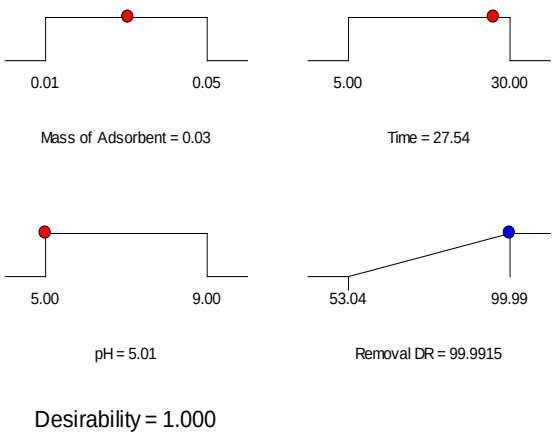


**Figure 9.** Graphs the optimum conditions for adsorption azo dye DR 278

**Table 6.** The BBD for the 4 independent variables

| STD | Run | Mass of adsorption (g) | Time (min) | pH | Removal Ni (%) |
|---|---|---|---|---|---|
| 1 | 1 | 0.01 | 5.00 | 7.00 | 62.32 |
| 7 | 2 | 0.01 | 17.50 | 9.00 | 65.38 |
| 3 | 3 | 0.01 | 30.00 | 7.00 | 75.32 |
| 8 | 4 | 0.05 | 17.50 | 9.00 | 77.43 |
| 15 | 5 | 0.03 | 17.50 | 7.00 | 81.22 |
| 12 | 6 | 0.03 | 30.00 | 9.00 | 80.29 |
| 4 | 7 | 0.05 | 30.00 | 7.00 | 97.43 |
| 10 | 8 | 0.03 | 30.00 | 5.00 | 57.11 |
| 13 | 9 | 0.03 | 17.50 | 7.00 | 82.81 |
| 6 | 10 | 0.05 | 17.50 | 5.00 | 50.98 |
| 9 | 11 | 0.03 | 5.00 | 5.00 | 46.97 |
| 14 | 12 | 0.03 | 17.50 | 7.00 | 81.94 |
| 5 | 13 | 0.01 | 17.50 | 5.00 | 52.76 |
| 2 | 14 | 0.05 | 5.00 | 7.00 | 70.23 |
| 11 | 15 | 0.03 | 5.00 | 9.00 | 71.33 |

**Table 7.** Results of analysis of variance in Ni (II)

| Source | Sum of squares | Degree of freedom | Mean square | F-value | P-value Prob >F |
|---|---|---|---|---|---|
| Model | 3234.23 | 9 | 359.36 | 81.34 | < 0.0001 significant |
| A-Mass | 285.61 | 1 | 285.61 | 64.64 | |
| of Adsorbent | 403.42 | 1 | 403.42 | 91.31 | 0.0005 |
| B-Time | 1699.74 | 1 | 1699.7 | 384.72 | 0.0002 |
| C-pH | 0.73 | 1 | 4 | 0.17 | < |
| AB | 286.12 | 1 | 0.73 | 64.76 | 0.0001 |
| AC | 19.45 | 1 | 286.12 | 4.40 | 0.7010 |
| BC | 67.87 | 1 | 19.45 | 15.36 | 0.0005 |
| A2 | 74.77 | 1 | 67.87 | 16.92 | 0.0900 |
| B2 | 452.06 | 1 | 74.77 | 102.32 | 0.0112 |
| C2 | 22.09 | 5 | 452.06 | 10.95 | 0.0092 |
| Residual | 20.82 | 3 | 4.42 | | 0.0002 |
| Lack of Fit | 1.27 | 2 | 6.94 | | |
| Pure Error | 3256.32 | 14 | 0.63 | | 0.0848 not |
| Cor Total | | | | | significant |

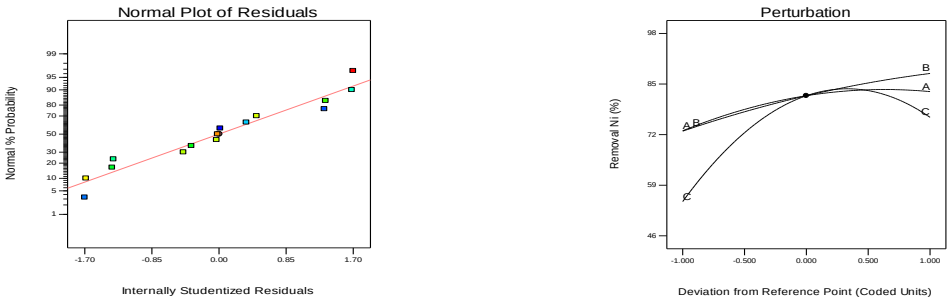


(a) (b)

**Figure 10. a)** Normal probability plot of the studentized residual for adsorption Ni(II) and **b)** Perturbation plot for adsorption Ni(II).

*The effect of adsorbent mass and time on the adsorption Ni (II) ion*

At this stage of the experiments, the effect of simultaneous changes of the two parameters of adsorbent mass and time on the efficiency of Ni (II) ion removal was investigated by considering the dye concentration of DR278 at 10 mg/L. Figure 11a and b show the effect of adsorbent mass and time on Ni (II) ion removal (2D and D). Based on the results, the removal efficiency increases with increasing adsorbent mass and time. The $MoS_2$/O-MWCNTS adsorbent is able to remove Ni (II) ions from water in a shorter period of time than other adsorbents. It can be said with confidence that this amount of adsorbent has the ability to remove more than 90% of the Ni (II) ion at extremely high concentrations of 100 mg/L.

*The effect of adsorbent mass and pH on the adsorption Ni (II) ion*

The pH value plays an important role in the adsorption of particle ions by the $MoS_2$/O-MWCNTS adsorbent. The pH is strongly dependent on the surface charge of the particles due to the binding of cations to the surfactants; it is one of the most important control parameters of the adsorption process. The pH affects the reaction between the adsorbent and the adsorbate by changing the ionic state of the metals, ionizing and charging the adsorbent surface. Figure 11c and d show the effect of adsorbent mass and pH on Ni (II) removal as a 2D and 3D. Based on the results, with increasing adsorbent mass and pH, the Ni (II) ion removal efficiency increases. The results of this study showed the $MoS_2$/O-MWCNTS adsorbent is in the neutral pH range and has a higher ability to remove Ni (II). The surface charge of the $MoS_2$ O-MWCNTS adsorbent becomes more negative with increasing pH, which in turn causes electrostatic reactions As a result, positively charged metal ions such as Ni (II)l are better adsorbed, Ni(II) precipitates when the pH of the solution rises above 7, and adsorption efficiency decreases, but when the pH of the solution is lower than $pH_{PZC}$ under acidic conditions at the charge-adsorbing surface. It is positive that it is effective in the adsorption of anionic species. Also, when the solution pH is higher than 7, Ni (II) precipitates and adsorption efficiency decreases, so it can be concluded that Ni (II) ions are well removed by the adsorbent in the neutral pH range.

*The effect of time and pH on the adsorption Ni (II) ion*

Figure shows the effect of time and pH on nickel removal as a 2D and 3D. Based on the results, the Ni (II) ion removal efficiency increases with increasing time and pH, as shown in Figure 11 e) and f). In the early stages, the adsorption rate was so high that more than 50% of the Ni (II) ion was separated from the solution within 5 min. The experiments lasted up to 30 min and the results showed that over time, the adsorption capacity increased but the adsorption intensity decreased.

*Determining the optimal conditions on the adsorption Ni (II) ion*

Finally, the software determined the best point to achieve the highest nickel ion removal efficiency (II), in the optimal conditions of adsorbent mass 0.04 (g), time 26.61 (min) and pH 7.09, 97.83%. Also, under the optimal conditions, the experiment was performed and the amount of nickel (II) ion removal efficiency was 97.61% (Figure 12).

*Isotherm models in adsorption of DR278 and Ni (II) ion*

One of the important pillars in adsorption studies is finding one or more suitable isotherms to analyze and present the adsorption experimental results. Several isothermal models have been proposed to analyze and present the experimental results of adsorption experiments, which are shown in Table 8. Here it is enough to mention the parameters of the models used to introduce the experimental results of adsorption experiments in this research.

Isothermal studies showed that the Dubinin–Radushkevich equation with the highest correlation coefficients of 0.97 and 0.98 for DR278 and Ni (II) ion with the lowest error rate has the highest agreement with the experimental data.

*Adsorption kinetics in adsorption of DR278 and Ni (II) ion*

To evaluate the adsorption kinetics of DR278 and Ni (II) ions on the $MoS_2$/O-MWCNTS adsorbent, the Lagergren, Elovich, Blanchard, and intraparticle diffusion control kinetic models were fitted with experimental data, the results of which are shown in Table 9. The results showed that among the kinetic equations, the Blanchard kinetic equation with the highest correlation coefficient had the highest agreement with the experimental data.

*Thermodynamics study in adsorption of DR278 and Ni (II) ion*

In this research, adsorption experiments at temperatures of 228, 298, 309, 318 and 328 K under optimal conditions obtained for DR278 and Ni (II) dyes are the values of $q_e$, $C_e$, K(T), LnK(T) and 1/T is the result of the performed experiments and can be calculated $\Delta G°_{ad}$ at any temperature from the equation $\Delta G°_{ad} = -RT\ lnK_{(T)}$. The thermodynamic functions are shown in Tables 10 and 11. Thermodynamic studies of DR278 adsorption on $MoS_2$/ O-MWCNTs adsorbent revealed that the adsorption studied under the applied conditions is warm $(\Delta H°_{ad} < 0)$ and spontaneous $(\Delta G°_{ad} < 0)$. and decreases. It is associated with "adsorption-adsorbate" system irregularities $(\Delta S°_{ad} < 0)$. The adsorption of Ni (II) ions on the $MoS_2$ /O-MWCNTs adsorbent revealed that the adsorption under the applied conditions is warm $(\Delta H°_{ad} < 0)$ and spontaneous, $(\Delta G°_{ad} < 0)$ and it is associated with a decrease in the irregularity of the" adsorption-adsorbate" system $(\Delta S°_{ad} < 0)$.

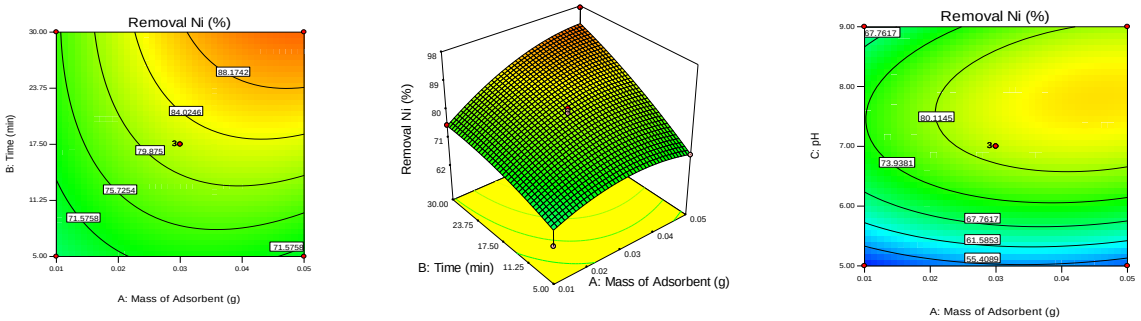


**(a)** **(b)** **(c)**

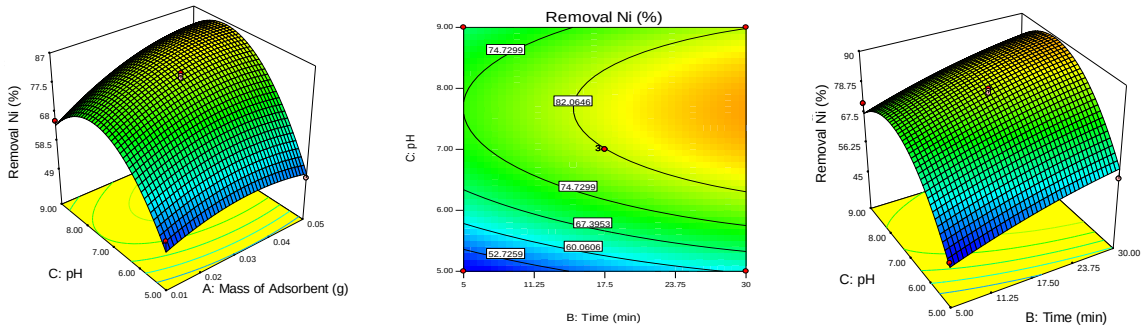


**(d)** **(e)** **(f)**

**Figure 11.** The effect of mass of adsorbent and time for adsorption Ni(II) a) Contour and b) 3D plot, the effect of mass of adsorbent and pH for adsorption Ni(II) c) Contour and d) 3D plot. The effect of time and pH for adsorption Ni(II) f) Contour and f) 3D plot.

**Table 8.** Isotherms and error functions for $MoS_2$/O-MWCNTs

| | | Ni (II) | | DR278 | |
|---|---|---|---|---|---|
| isotherms | Equation | Nonlinear isotherm parameter | Error Value & $R^2$ | Nonlinear isotherm parameter | Error Value & $R^2$ |
| Langmuir | $q_e = \frac{q_m \times b \times C_e}{1 + b \times C_e}$ | | | | |
| $q_m$ | | 248.4766 | 0.143 | 294.7014 | 0.251 |
| $b_L$ | | 0.1813 | $R^2$ =0.9389 | 1.8699 | $R^2$= 0.8889 |
| Freundlich | $q_e = k_f \times C_e^{1/n}$ | | | | |
| $K_f$ | | 91.4400 | 0.73 | 170.9290 | 0.255 |
| N | | 4.7195 | $R^2$ =0.9608 | | $R^2$ =0.8818 |
| Temkin | $q_e = B_T \times ln(A_T \times C_e)$ | | | | |
| $B_T$ | | 19.5184 | 0.0693 | 10.1605 | 0.0777 |
| $A_T$ | | 0.5230 | $R^2$ =0.9517 | | $R^2$ =0.9600 |
| Dubinin-Radushkevich | $q_e = \frac{K_R \times C_e}{1 + a_R \times C_e^g}$ | | | | |
| $q_s$ | | 71.9087 | 0.0087 | 117.1218 | 0.2994 |
| $K_{ad}$ | | 96.0703 | $R^2$ =0.9863 | 1.7298 | $R^2$ =0.9741 |
| E | | 0.0770 | | | |
| Redlich-Peterson | $q_e = \frac{K_R \times C_e}{1 + a_R \times C_e^g}$ | | | | |
| $K_R$ | | 204.3594 | 0.1260 | 375.3373 | 0.2502 |
| $a_R$ | | 1.8327 | $R^2$ =0.9632 | 0.8463 | $R^2$ =0.8926 |
| G | | 0.9695 | | | |

**Table 9.** Kinetic model for $MoS_2$/O-MWCNTs

| Kinetic model | General Formula | | | | |
|---|---|---|---|---|---|
| | | | $k_1$ | $q_e$ | $R^2$ |
| Logergern | $\ln(q_e - q_t) = lnq_e - k_1 t$ | DR278 | 0.0220 | 24.4291 | 0.9466 |
| | | Ni(II) | 0.0191 | 34.1882 | 0.9455 |
| | | | $A$ | $B$ | $R^2$ |
| Elovich | $q_t = \frac{1}{\beta}\ln(\alpha\beta) + \frac{1}{\beta}\ln(t)$ | DR278 | 1.06E+08 | 0.1450 | 0.9457 |
| | | Ni(II) | 116116.3 | 0.1037 | 0.9098 |
| | | | $k_2$ | $q_e$ | $R^2$ |
| Blanchard | $\frac{t}{q_t} = \frac{1}{k_2 q_e^2} + \frac{t}{q_e}$ | DR278 | 0.0021 | 150.8473 | 0.9947 |
| | | Ni(II) | 0.0013 | 143.291 | 0.9973 |
| | | | $k_i$ | $C$ | $R^2$ |
| Intra-particle diffusion control | $q_t = k_1 t^{\frac{1}{2}} + C$ | DR278 | 0.2993 | 131.6992 | 0.9793 |
| | | Ni(II) | 0.4307 | 114.8802 | 0.9979 |

**Table 10.** Thermodynamic parameters for the DR 278 adsorption on the $MoS_2$-O-MWCNTs adsorbent

| Temperature (K) | ΔG° (kJ mol$^{-1}$) | ΔH° (kJ mol$^{-1}$) | ΔS° (kJ mol$^{-1}$ k$^{-1}$) |
|---|---|---|---|
| 298 | -21.91 | -144.8 | -0.4 |
| 308 | -20.92 | | |
| 318 | -11.42 | | |
| 328 | -11.48 | | |

**Table 11.** Thermodynamic parameters for the Ni(II) adsorption on the $MoS_2$-O-MWCNTs adsorbent

| Temperature (K) | ΔG° (kJ mol$^{-1}$) | ΔH° (kJ mol$^{-1}$) | ΔS° (kJ mol$^{-1}$ k$^{-1}$) |
|---|---|---|---|
| 298 | -11.31 | -64 | -0.16 |
| 308 | -13.09 | | |
| 318 | -10.05 | | |
| 328 | -9.80 | | |

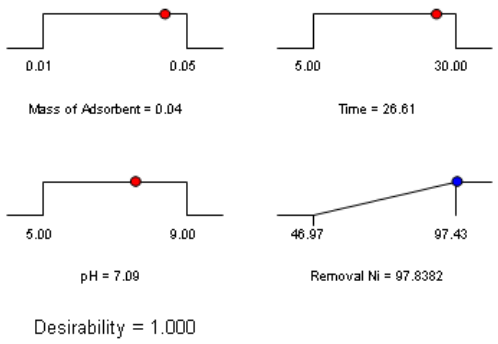


**Figure 12.** Graphs the optimum conditions for adsorption Ni (II).

## CONCLUSION

$MoS_2$ particles were also synthesized by the hydrothermal method and loaded on O-MWCNTs. $MoS_2$ and $MoS_2$/O-MWCNTs particles were characterized by different techniques. Removal of DR278 dye and Ni (II) ions was investigated by $MoS_2$ and $MoS_2$/O-MWCNTs particles. The RSM with BBD design with 3 variables was used to investigate the relationship between the obtained responses and process variables and optimize the combinations with Design Expert software. The effect of adsorbent mass (g), time (min) and pH was evaluated at three levels with two responses. Finally, the software determined the best point to achieve the highest removal efficiency for DR278 paint in the optimal conditions of adsorbent mass 0.03 g, time 27.54 min, and pH 5.01, which were found 99.99%. Also, the removal efficiency for Ni (II) ions, under optimal conditions of adsorbent mass of 0.04 g, time of 26.61 min and pH of 7.09 was found to be 97.83%. It is very important that the cost of effluent be affordable. In general, one of the key factors in choosing a method and type of adsorbent is its practicality, simplicity of design, and cost-effectiveness. The adsorption process provides these benefits and is suitable for removing paint from effluents. The studies of this research confirm the efficiency of the adsorption method with the help of adsorbent $MoS_2$/O-MWCNTs in wastewater treatment.

## REFERENCES

[1]. Hasanpour, M., & Hatami, M. Application of three dimensional porous aerogels as adsorbent for removal of heavy metal ions from water/wastewater: A review study. *Adv. Colloid Interface Sci*, 2020, p.102247.

[2]. Esrafili, L., Firuzabadi, F. D., Morsali, A., & Hu, M. L. Reuse of predesigned dual-functional metal organic frameworks (DF-MOFs) after heavy metal removal. *J. Hazard. Mater*, 2021, vol. 403, p.123696.

[3]. Wadhawan, S., Jain, A., Nayyar, J., & Mehta, S. K Role of nanomaterials as adsorbents in heavy metal ion removal from waste water: A review. *J. Water Process. Eng*, 2020, vol. 33, p.101038.

[4]. Ren, R. Y., Yang, L. H., Han, J. L., Cheng, H. Y., Ajibade, F. O., Guadie, A., ... & Wang, A. J. Perylene pigment wastewater treatment by fenton-enhanced biological process. Environ. Res, 2020, p.109522.

[5]. Aramesh, N., Bagheri, A. R., & Bilal, M. Chitosan-composite/hybrid biomaterials for adsorptive removal of dyes and underlying interaction mechanisms. *Int. J. Biol. Macromol*, 2021, vol 183, pp.399-422.

[6]. Zhuang, H., Shi, J., Shan, S., Ping, L., & Zhang, C. Enhanced anaerobic treatment of azo dye wastewater via direct interspecies electron transfer with $Fe_3O_4$/sludge carbon. *Int. J. Hydrog. Energy*, 2020, vol. 45, no. 53, p. 28476-28487.

[7]. Shokouhi, S. B., Dehghanzadeh, R., Aslani, H., & Shahmahdi, N. Activated carbon catalyzed ozonation (ACCO) of Reactive Blue 194 azo dye in aqueous saline solution: Experimental parameters, kinetic and analysis of activated carbon properties. *J. Water Process. Eng*, 2020, vol. 35, p. 101188.

[8]. Kwon, G., Cho, D. W., Wang, H., Bhatnagar, A., & Song, H. Valorization of Plastics and Paper Mill Sludge into Carbon Composite and its Catalytic Performance for Azo Dye Oxidation. *J. Hazard. Mater*, 2020, p.123173.

[9]. Fard, N. E., & Fazaeli, R. A novel kinetic approach for photocatalytic degradation of azo dye with CdS and Ag/CdS nanoparticles fixed on a cement bed in a continuous-flow photoreactor. *Int. J. Chem. Kinet*, 2016, vol. 48, no. 11, pp. 691-701.

[10]. Fard, N. E., Fazaeli, R., & Ghiasi, R. Band gap energies and photocatalytic properties of CdS and Ag/CdS nanoparticles for Azo dye degradation. Chem. Eng. Technol, 2016, vol. 39, no. 1, pp. 149-157.

[11]. Biju, L. M., Pooshana, V., Kumar, P. S., Gayathri, K. V., Ansar, S., & Govindaraju, S. Treatment of

textile wastewater containing mixed toxic azo dye and chromium (VI) BY haloalkaliphilic bacterial consortium. Chemosphere, 2022, vol. 287, p.132280.

[12]. Nekooie, R., Shamspur, T., & Mostafavi, A. Novel CuO/$TiO_2$/PANI nanocomposite: Preparation and photocatalytic investigation for chlorpyrifos degradation in water under visible light irradiation. *J. Photochem. Photobiol*, 2021, vol. 407, p.113038.

[13]. Alardhi, S. M., Albayati, T. M., & Alrubaye, J. M. Adsorption of the methyl green dye pollutant from aqueous solution using mesoporous materials MCM-41 in a fixed-bed column. *Heliyon*, 2020, vol. 6, no. 1, p. e03253.

[14]. Staciwa, P., Sibera, D., Pełech, I., Narkiewicz, U., Łojkowski, W., Dąbrowska, S., & Cormia, R. Effect of microwave assisted solvothermal process parameters on carbon dioxide adsorption properties of microporous carbon materials. *Microporous and Mesoporous Mater*, 2020, vol. 314, p. 110829.

[15]. Santana-Viera, S., Padrón, M. E. T., Sosa-Ferrera, Z., & Santana-Rodríguez, J. J. Quantification of cytostatic platinum compounds in wastewater by inductively coupled plasma mass spectrometry after ion exchange extraction. *Microchem. J*, 2020, vol. 157, p. 104862.

[16]. Kalla, S. Use of membrane distillation for oily wastewater treatment–a review. *J. Environ. Chem. Eng*, 2021, vol. 9, p.104641.

[17]. Alvial-Hein, G., Mahandra, H., & Ghahreman, A. Separation and recovery of cobalt and nickel from end of life products via solvent extraction technique: A review. 2021, *J. Clean. Prod*, vol.297, p. 126592.

[18]. Martínez-Huitle, C. A., & Panizza, M. Electrochemical oxidation of organic pollutants for wastewater treatment. *Curr. Opin. Electrochem*, 2018, vol. 11, pp. 62-71.

[19]. Peng, H., & Guo, J. Removal of chromium from wastewater by membrane filtration, chemical precipitation, ion exchange, adsorption electrocoagulation, electrochemical reduction, electrodialysis, electrodeionization, photocatalysis and nanotechnology: a review. *Environ. Chem. Lett*, 2020, pp. 1-14.

[20]. Ahangaran, E., Aghaie, H., & Fazaeli, R. Study of Amoxicillin Adsorption on the Silanized Multiwalled Carbon Nanotubes: Isotherms, Kinetics, and Thermodynamics Study. Russ. J. Physic. Chem. A, 2020, vol. 94, no. 13, pp. 2818-2828.

[21]. Donkadokula, N. Y., Kola, A. K., Naz, I., & Saroj, D. A review on advanced physico-chemical and biological textile dye wastewater treatment techniques. *Rev. Environ. Sci. Biotechnol*. 2020, pp.1-18.

[22]. Elmi Fard, N., & Fazaeli, R. Experimental design study of RB 255 photocatalytic degradation under visible light using synthetic Ag/$TiO_2$ nanoparticles: Optimization of experimental conditions. *Iran. J. Catal*, 2018, vol. 8, no. 2, pp. 133-141.

[23]. Fard, N. E., & Fazaeli, R. Optimization of Operating Parameters in Photocatalytic Activity of Visible Light Active Ag/$TiO_2$ Nanoparticles. *Russ. J. Physic. Chem. A*, 2018, vol. 92, no. 13, pp. 2835-2846.

[24]. Fard, N. E., Fazaeli, R., Yousefi, M., & Abdolmohammadi, S. Oxidation of carbazole by shape-controllable $Cu_2O$ on MWW catalysis. *Appl. Physic. A*, 2019, vol. 125, no. 9, pp. 632.

[25]. Fard, N. E., Fazaeli, R., Yousefi, M., & Abdolmohammadi, S. Morphology-Controlled Synthesis of CuO, CuO Rod/MWW Composite for Advanced Oxidation of Indole and Benzothiophene. *Chem. Select*, 2019, vol. 4, no. 33, pp. 9529-9539.

[26]. Adityosulindro, S., Julcour, C., & Barthe, L. Heterogeneous Fenton oxidation using Fe-ZSM5 catalyst for removal of ibuprofen in wastewater. *J. Environ. Chem. Eng*, 2018, vol. 6. no. 5, pp. 5920-5928.

[27]. Dehghani, M. H., Kamalian, S., Shayeghi, M., Yousefi, M., Heidarinejad, Z., Agarwal, S., & Gupta,

V. K. High-performance removal of diazinon pesticide from water using multi-walled carbon nanotubes. *Microchem J*, 2019, vol. 145, pp. 486-491.

[28]. Wang, Z., Sim, A., Urban, J. J., & Mi, B. Removal and recovery of heavy metal ions by two-dimensional MoS2 nanosheets: performance and mechanisms. Environ. Sci. Technol, 2018, vol. 52, no. 17, pp. 9741-9748.

[29]. Wang, Z., & Mi, B. Environmental applications of 2D molybdenum disulfide (MoS2) nanosheets. Environmental science & technology, 2017, vol. 51, no. 15, pp. 8229-8244.

[30]. Zhao, H., Mu, X., Zheng, C., Liu, S., Zhu, Y., Gao, X., & Wu, T. Structural defects in 2D MoS2 nanosheets and their roles in the adsorption of airborne elemental mercury. J. Hazard. Mater, 2019, vol. 366, pp. 240-249.

[31]. Kashi, N., Fard, N. E., & Fazaeli, R. Empirical modeling and CCD-based RSM optimization of Cd (II) adsorption from aqueous solution on clinoptilolite and bentonite. Russ. J. Appl. Chem, 2017, vol. 90, no. 6, pp. 977-992.

[32]. Fazaeli, R., & Fard, N. E. Desulfurization of Gasoline Fuel via Photocatalytic Oxidation/Adsorption Using NaX Zeolite-Based under Mild Conditions: Process Optimization by Central Composite Design. Russ. J. Appl. Chem, 2020, vol. 93, no. 7, pp. 973-982.

[33]. Fekr, S. S., Fard, N. E., & Fazaeli, R. Erratum to: Photocatalytic Degradation of Antibiotic Norfloxacin Aqueous Solution by Ce/$Bi_2WO_6$: Optimization and Simulation of Process by RSM. *Russ. J. Appl. Chem*, 2021, vol. 94 no. 7, pp.1009-1009.

[34]. Saadi, R., Saadi, Z., Fazaeli, R., & Fard, N. E. Monolayer and multilayer adsorption isotherm models for sorption from aqueous media. *Korean. J. Chem. Eng*, 2015, vol. 32, no. 5, pp. 787-799.

[35]. Vandani, S. A. K., Fazaeli, R., Saravani, M. G., & Pasdar, H. Preparation of Ni/CuO/MCM-41 for indole oxidation: optimisation processes. *J. Environ. Eng. Sci*. 2021, vol. 17, no. 1, pp.10-20.

[36]. Vandani, S. A. K., Fazaeli, R., Giahi Saravani, M., & Pasdar, H. Cu (II)/Z4A as an Efficient Nanocomposite for Oxidative Degradation of Indole and Optimization of Effective Factors via RSM Procedure. *Egypt. J. Chem*., 2021, vol. 64, no. 10, pp. 3-4.